Journal of Coastal Research	20	1	70–88	West Palm Beach, Florida	Winter 2004

Ship Shoal as a Prospective Borrow Site for Barrier Island Restoration, Coastal South-Central Louisiana, USA: Numerical Wave Modeling and Field Measurements of Hydrodynamics and Sediment Transport

Gregory W. Stone†, David A. Pepper‡, Jingping Xu§ and Xiongping Zhang†

†Coastal Studies Institute and Department of Oceanography and Coastal Sciences
Louisiana State University
Baton Rouge, LA 70803, USA

‡Present Address:
Department of Geography
University of Southern California
Los Angeles, CA 90089, USA

§U.S. Geological Survey
Menlo Park, CA 94025, USA

ABSTRACT

STONE, G.W.; PEPPER, D.A.; XU, J., and ZHANG, X., 2004. Ship Shoal as a prospective borrow site for barrier island restoration, coastal south-central Louisiana, USA: numerical wave modeling and field measurements of hydrodynamics and sediment transport. *Journal of Coastal Research,* 20(1), 70–89. West Palm Beach (Florida), ISSN 0749-0208.

Ship Shoal, a transgressive sand body located at the 10 m isobath off south-central Louisiana, is deemed a potential sand source for restoration along the rapidly eroding Isles Dernieres barrier chain and possibly other sites in Louisiana. Through numerical wave modeling we evaluate the potential response of mining Ship Shoal on the wave field. During severe and strong storms, waves break seaward of the western flank of Ship Shoal. Therefore, removal of Ship Shoal (approximately 1.1 billion m^3) causes a maximum increase of the significant wave height by 90%–100% and 40%–50% over the shoal and directly adjacent to the lee of the complex for two strong storm scenarios. During weak storms and fair weather conditions, waves do not break over Ship Shoal. The degree of increase in significant wave height due to shoal removal is considerably smaller, only 10%–20% on the west part of the shoal. Within the context of increasing nearshore wave energy levels, removal of the shoal is not significant enough to cause increased erosion along the Isles Dernieres. Wave approach direction exerts significant control on the wave climate leeward of Ship Shoal for stronger storms, but not weak storms or fairweather. Instrumentation deployed at the shoal allowed comparison of measured wave heights with numerically derived wave heights using STWAVE. Correlation coefficients are high in virtually all comparisons indicating the capability of the model to simulate wave behavior satisfactorily at the shoal.

Directional waves, currents and sediment transport were measured during winter storms associated with frontal passages using three bottom-mounted arrays deployed on the seaward and landward sides of Ship Shoal (November, 1998–January, 1999). Episodic increases in wave height, mean and oscillatory current speed, shear velocity, and sediment transport rates, associated with recurrent cold front passages, were measured. Dissipation mechanisms included both breaking and bottom friction due to variable depths across the shoal crest and variable wave amplitudes during storms and fair-weather. Arctic surge fronts were associated with southerly storm waves, and southwesterly to westerly currents and sediment transport. Migrating cyclonic fronts generated northerly swell that transformed into southerly sea, and currents and sediment transport that were southeasterly overall. Waves were 36% higher and 9% longer on the seaward side of the shoal, whereas mean currents were 10% stronger landward, where they were directed onshore, in contrast to the offshore site, where seaward currents predominated. Sediment transport initiated by cold fronts was generally directed southeasterly to southwesterly at the offshore site, and southerly to westerly at the nearshore site. The data suggest that both cold fronts and the shoal, exert significant influences on regional hydrodynamics and sediment transport.

ADDITIONAL INDEX WORDS: *Cold fronts, currents, inner shelf, storms, Gulf of Mexico.*

INTRODUCTION

Erosion of both barrier islands and wetlands in coastal Louisiana is occurring at rates largely unreported elsewhere around the globe (see reviews in STONE *et al.,* 1997; WILLIAMS *et al.,* 1997). Large-scale barrier island restoration will likely prove a major contributor to mitigating the wave field in Louisiana's bays and, therefore, reduce incident wave energy along fringing marshes resulting in a considerable reduction in wetland loss (STONE and MCBRIDE, 1998). Although billions of cubic meters of sand will be required for initial and recurring restoration, high quality sand is largely limited to isolated shoals or infilled fluvial channels on the inner shelf. One such deposit, Ship Shoal, lays at the 10-m isobath in south-central Louisiana adjacent a rapidly eroding barrier island complex, the Isles Dernieres (Figure 1). Here we summarize the results of a comprehensive program funded by the Minerals Management Service (MMS) and con-

6 received and accepted in revision 6 June 2003.

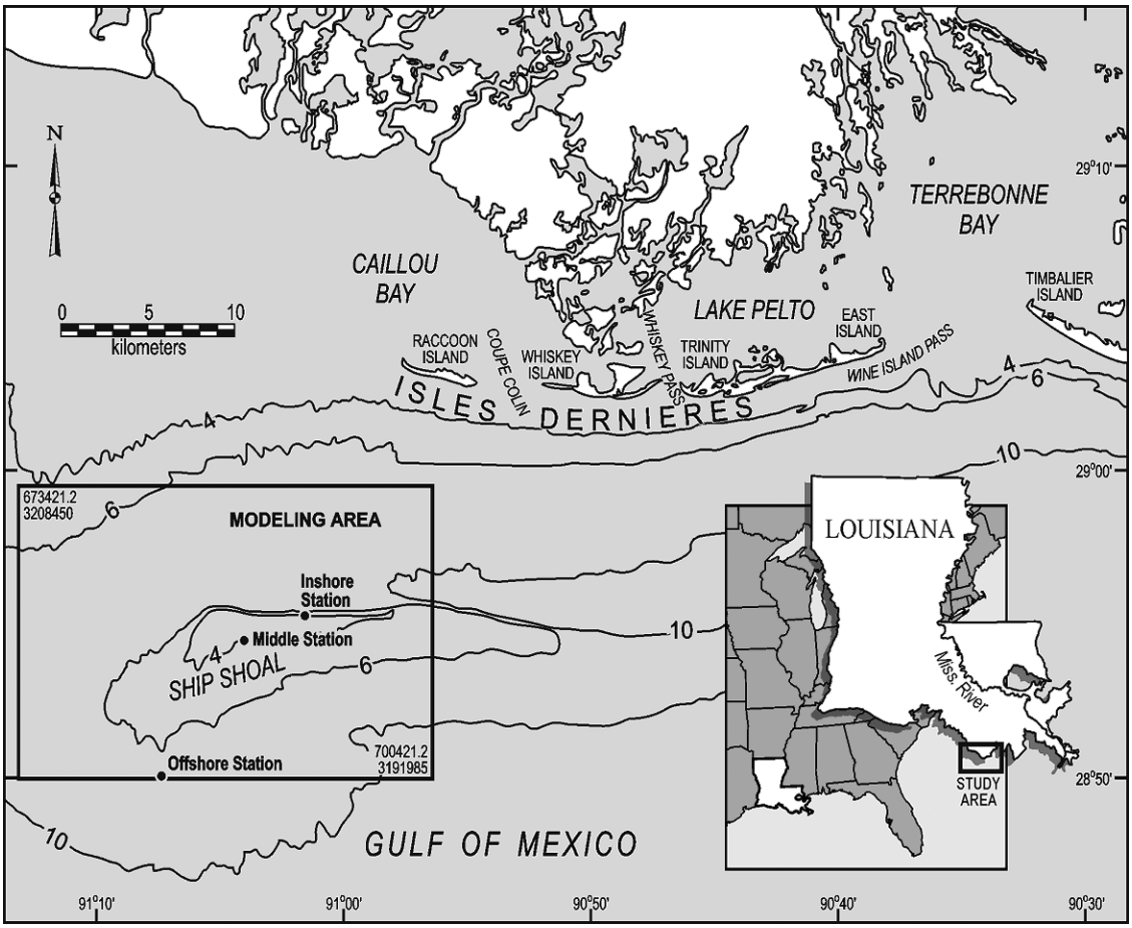

Figure 1. Map of the study site including the Isles Dernieres located in south-central Louisiana, and Ship Shoal on the 10-m isobath. The rectangle delimits the area modeled and the location of three sites where instruments were deployed.

ducted by scientists in the Coastal Studies Institute, Louisiana State University, to evaluate physical processes and sediment transport at Ship Shoal. The first part of the paper summarizes the extent of the problem and reviews the literature pertinent to barrier restoration and sand mining. The second part documents a detailed numerical wave modeling effort designed to assess the potential impacts of removing Ship Shoal through dredging on the wave field. The third part deals with a physical measurement program also funded by MMS which focuses on measuring bottom boundary layer parameters and sediment transport at the shoal. These data also provide an opportunity to compare in situ measurements with numerically derived wave information.

BACKGROUND

It is well established in the literature that barrier islands in south-central Louisiana (Figure 1) have been experiencing among the highest rates of shoreline retreat in the United States (McBride *et al.,* 1992; Stone and Penland, 1992; Williams *et al.,* 1992; Stone *et al.,* 1997; Williams *et al.,* 1997). The primary factors responsible for deterioration of these islands includes (1) eustatic sea-level rise; (2) compactional and geological subsidence; (3) wave erosion; (4) wind deflation; (5) reduction in sediment supply and (6) anthropogenic activity (*e.g.,* river diversion, dredging, levee building and maintenance). Historical erosion rates along the Isles Dernieres ranged from 4.8 m/yr (East Island) to 22.9 m/yr (Wine Island) over the last century or so (McBride *et al.,* 1992). Recent evidence indicates an apparent acceleration in erosion, approximating 213% over the last decade (Williams *et al.,* 1992). Based on these data, it is estimated that several of the islands will disappear within the next decade or two (McBride *et al.,* 1992; McBride and Byrnes, 1997; Stone and McBride, 1998). Given the recent impact of Hurricane Andrew and various tropical cyclones along this coast (Stone *et al.,* 1993; Stone *et al.,* 1995; Grymes and Stone, 1995; Muller and Stone, 2002), it is probable that this time period is less.

With the degradation of barrier systems, it is likely that mainland shoreline erosion and wetland loss will occur in response to a more energetic, local wave field (Penland and Suter, 1988; McBride *et al.,* 1992)—although, the critical

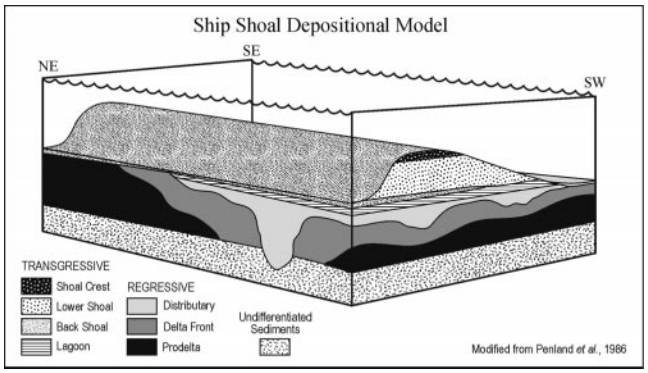

Figure 2. Depositional model of Ship Shoal showing the various transgressive and regressive facies and underlying undifferentiated sediments (modified from PENLAND *et al.,* 1996).

links have not yet been fully investigated (LIST and HANSEN, 1992; STONE and MCBRIDE, 1998). Recent data indicate that land loss in the Terrebonne Bay area averaged 0.86 km^2/yr between 1932 and 1990 (BRITSCH and DUNBAR, 1993). Approximately 12 million m^3 of sand would be required to restore the Isles Dernieres to a configuration indicative of the late 1800's. Several studies, funded largely by MMS, indicate the potential use of Ship Shoal (Figure 1) as a source of clean quartz sand (approximately 1.2 billion m^3) for barrier island restoration along Isles Dernieres (MOSSA, 1988). Dredging of the material appears both technically and economically feasible (BYRNES and GROAT, 1991), and a detailed evaluation of the potential alteration of physical and sedimentary processes associated with using Ship Shoal as a source began in the mid 1990's. The data presented here build on the findings of MOSSA (1988), and BYRNES and GROAT (1991) which pertained to evaluating changes to wave refraction patterns, and qualitative assessments of the resultant wave energy distribution along the Isles Dernieres due to partial dredging of Ship Shoal.

SITE DESCRIPTION AND REGIONAL SETTING

The study site is located off the south-central Louisiana coast (Figure 1). The morphology of the study area is the product of a process combining relative sea-level rise with regressive (delta building) sequences, and transgressive (delta abandoning) sequences of the Mississippi River (PENLAND *et al.,* 1985; 1986; COLEMAN *et al.,* 1998). Over the last 7,000 years, the Mississippi River has built six major delta lobes (FRAZIER, 1967). Except for the Modern delta and Atchafalaya delta complexes, all other abandoned deltas have responded to the Holocene transgression by undergoing erosion, subsidence, sediment redistribution, and landward migration. Isle Dernieres, Timbalier islands, and Ship Shoal are all products of these processes. Ship Shoal is a transgressive sand deposit located 15 km offshore of Isles Dernieres near the 10 m isobath, and was formed by the erosion of a submerged barrier system. The shoal is approximately 50 km long, varies in width from 2 to 10 km as delineated by the 6 m isobath, and is comprised of well-sorted, clean quartz sand, and is the easternmost member of a group of Holocene inner shelf shoals located southwest of the Mississippi River delta plain (PENLAND *et al.,* 1986). Bathymetric comparisons covering a time span of over a century since 1853 indicate that Ship Shoal has migrated landward by approximately 1.5 km (PENLAND *et al.,* 1986; LIST *et al.,* 1997).

Table 1. *Sources of wave climate data.*

Sources	Lat. (N)	Long. (W)	Water Depth (m)
WIS 19	28.5°	91.0°	33
WIS 20	28.5°	90.5°	38
WIS 21	28.5°	90.0°	91
NDBC 42017	27.5°	90.5°	407
LATEX 16	28.9°	90.5°	21

PENLAND *et al.* (1986) identified seven major sedimentary facies in the study area and its vicinity based on lithology, texture, sedimentary structures, faunal assemblages and stratigraphic position. A block diagram illustrating shoal facies and depositional environment (PENLAND *et al.,* 1986) is shown in Figure 2. Of the seven facies, the first three are the most significant with regards to characterization of the surficial sediment and the environments of deposition. The first facies (shoal crest), representing the crest of Ship Shoal, is located within the upper 5 m of the shoal and is characterized as a very well-sorted, well-rounded 99% quartz sand that coarsens upward within the unit from 0.13 mm at the base to about 0.16 mm at the top. The second facies (lower shoal), which represents the central body or shoal front of Ship Shoal, is a 1.2 to 3.4 m thick, moderately sorted and very fine to fine (0.12 to 0.15 mm), sand that underlies facies 1. Facies 3 (back shoal) is characterized by poorly sorted, very fine sand (0.1 to 0.13 mm), with interbedded layers of silty clay. It represents the lower extent, or shoal base, of Ship Shoal. The shoal crest contains 112 million cubic meters of sand and resides within the zone of active fairweather and storm wave processes. Water depths over the shoal crest range from 2.7 m along the west to 7.0 m along the east. The shoal front and shoal base environments contain approximately 430 and 640 million m^3 of sand respectively. Because these two facies are in deeper water, they are subjected to a lower wave energy environment.

MODELLING POTENTIAL CHANGES IN WAVE FIELD DUE TO SAND MINING

Numerical Models

Projects have yet to be designed for barrier restoration using Ship Shoal sand. Thus it remains unclear as to precisely how much sand would be required from Ship Shoal for future barrier restoration projects. Efforts to numerically model potential changes to wave processes as a consequence of shoal mining have largely focused on entire shoal removal. Several numerical models exist with the general capabilities of wave height prediction from deep water to the break point. These models define the wave field as monochromatic or single-period waves, one-dimensional spectral waves, two-dimensional spectral waves, or shallow water waves. As presented earlier, the objectives of wave modeling in this project are two-fold: (1) large-

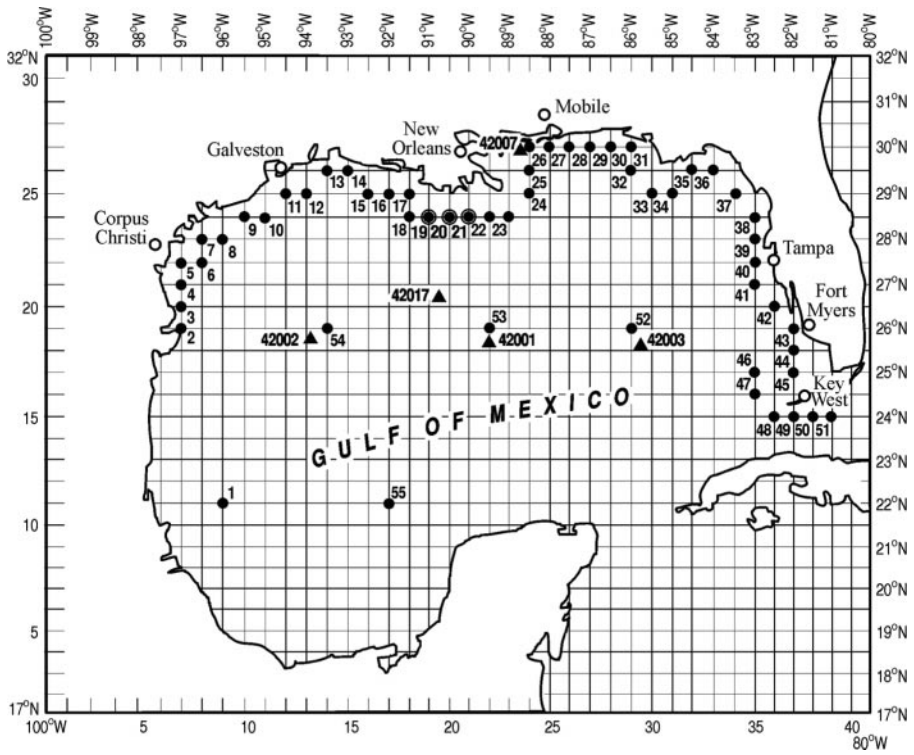

Figure 3. Distribution of Wave Information Study sites in the Gulf of Mexico represented by black circles. WIS 19, 20, and 21 were used in this study. Location of three National Data Buoy Center buoys are shown in black triangles. NDBC 42001 and 42017 were used in this study.

scale (or global scale) modeling that provides wave characteristics across the south-central Louisiana shelf, including the study area; and (2) local wave modeling that outputs higher resolution information (*e.g.* wave breaking) to evaluate the potential impacts of shoal removal on nearshore wave conditions. In this paper, we concentrate on the latter objective; the complete evaluation can be found in STONE and XU (1996), and STONE (2000). Additional model reviews may be found in HOLTHUIJSEN *et al.* (1989); O'REILLY and GUZA (1993).

Model Selection

As discussed in STONE and XU (1996), and STONE (2000), four models (RCPWAVE, STWAVE, REF/DIF 1 and REF/DIF S were compared against the following criteria: representation (scale), efficiency, accuracy, spectral capability, computational grid size requirement, breaking criteria, and wind-wave generating ability. STWAVE had the highest composite score because of its spectral capability, inclusion of a wind-forcing function, high accuracy, and high efficiency. Given the objectives presented earlier, STWAVE was selected for use in this study.

Table 2. *Incident wave parameters used for deep water wave boundary conditions.*

Scenario	H_s (m)	T_p (s)	Approach Dir. (deg.)[1]	Description
1	6	11	−45,00, +45	Severe Storm
2	4	9	−45,00, +45	Strong Storm
3	2	6	−45,00, +45	Weak Storm
4	1	5	−45,00, +45	Fairweather

[1] −45 = southwest approach; 45 = southeast approach; 00 = south approach.

Boundary Conditions

Computational bathymetric grids and deep water wave conditions (directional amplitude and period weighted by frequency of occurrence) are necessary inputs for numerical modeling of surface wave behavior across the study site. Three different types of bathymetric grid were generated for application in this study. The grids differed in resolution, and underwent embedding of "local" (high resolution) in "global" (coarser resolution) grids. A quantitative inventory and assessment of the wave climate in the vicinity of the study area is presented in addition to quantification of wave parameters at the offshore boundary of the computational grids.

Deep Water Database for Winter Storms and Fairweather

Deep water wave inputs representing winter storms and fairweather conditions were obtained from three sources (Table 1): (1) 20 years (1956–1975) of hindcast data obtained from the Wave Information Study (WIS) (ABEL *et al.,* 1989; HUBERTZ and BROOKS, 1989); (2) National Oceanic and Atmospheric Administration (NOAA)'s National Data Buoy Center (NDBC) buoy 42017 (25.9°N, 89.7°W); and (3) Loui-

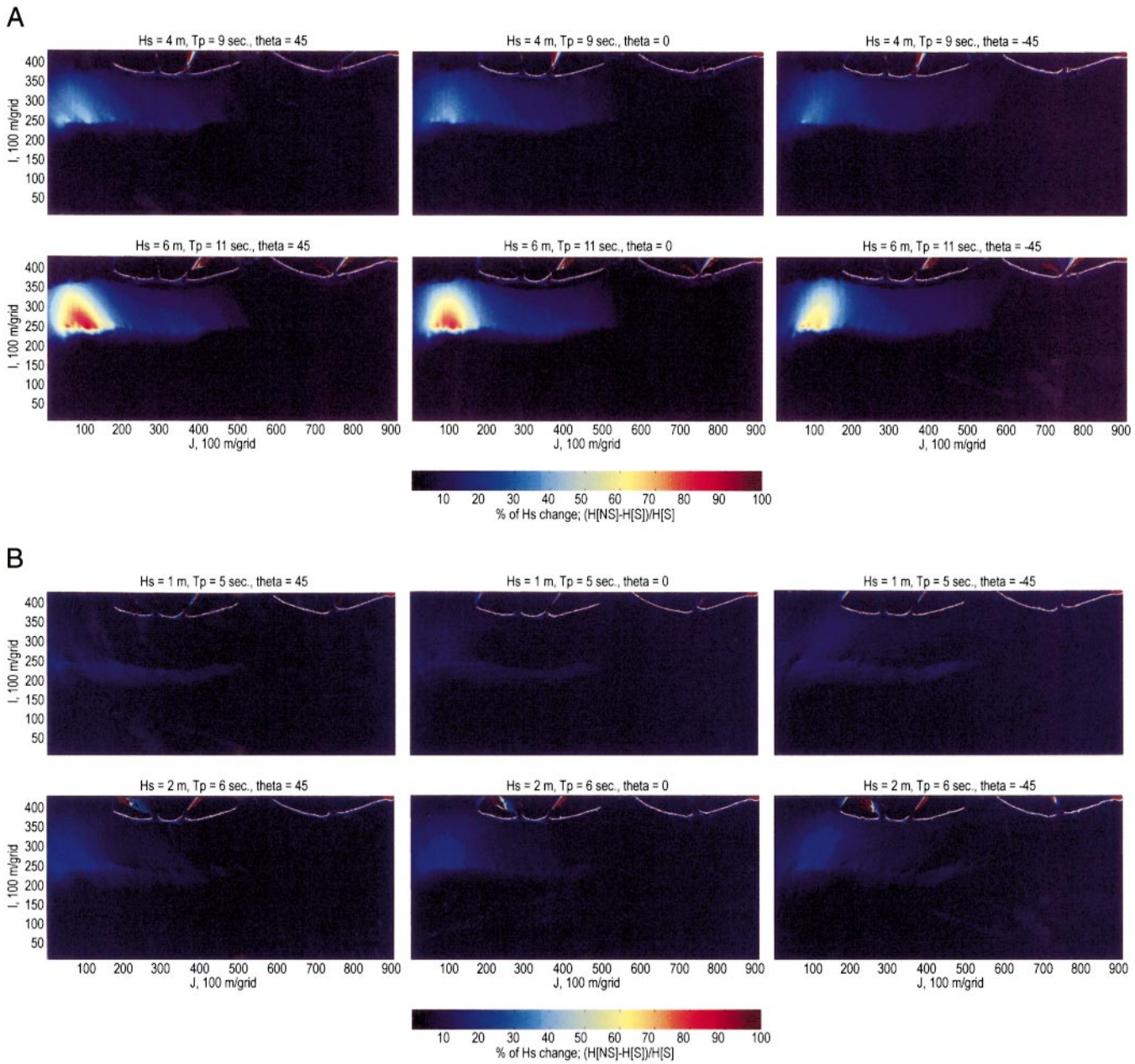

Figure 4. (A) Percentage increase in numerically derived significant wave height on comparing output with and without Ship Shoal in the computational grid. Upper panels represent moderate storm wave conditions for three directions of wave approach (southeast, south and southwest respectively). Lower panels represent percent increase in wave height using a deep water wave height indicative of a strong storm. The Isles Dernieres are located at the top of each diagram for reference.

Figure 4. (B) Percentage increase in numerically derived significant wave height on comparing output with and without Ship Shoal in the computational grid. Upper panels represent fair-weather wave conditions for three directions of wave approach (southeast, south and southwest respectively). Lower panels represent percent increase in wave height using a deep water wave height indicative of a weak storm. The Isles Dernieres are located at the top of each diagram for reference.

siana-Texas Shelf Physical Oceanography Program (LATEX) station 16 (28.9°N, 90.5°W; unpublished data supplied by Dr. Steven F. DiMarco, Texas A&M University).

Among the three sources, the WIS data set provides the most complete information. Statistics from three hindcast stations 19, 20, and 21 (Figure 3 for location) had shown an annual-mean significant wave height of 1.0 ± 0.2 m and mean peak period of 4.5–6.0 sec. The maximum wave heights from these stations exceeded 5 m, and the peak period associated with the largest wave exceeded 11 sec. The monthly mean

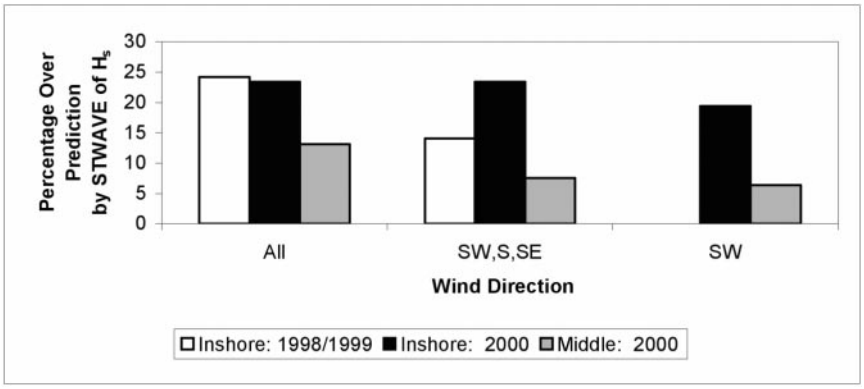

Figure 5. Summary of percent over prediction of H_s by STWAVE for all stations.

significant wave heights in winter (Dec.–Mar.) were 0.2–0.6 m higher than that of the rest of the year. The predominant wave directions were from the Southeastern quadrant (135.0°, 112.5°, and 90.0° for Stations 19, 20 and 21 respectively). The average directions associated with the largest waves were also mostly from this quadrant (125°, 117°, and 112° for the three stations). On summing the percentages of occurrence of wave directions in the range of 90°–180°, the percentages for the four stations are 76%, 85%, and 85% respectively.

Among the buoys that NDBC have administered within the Gulf of Mexico, 42017 (27.5°N, 90.5°W) is more significant for the purpose of the current project because of its close location to the study area (Figure 3). However, only 6 months (Apr.–Sep. 1989) of data were available from NDBC 42017. Although limited, the time series shows that the monthly mean significant wave heights ranged from 0.6 to 1.4 m and peak periods from 4.5 to 5.3 sec. A storm at the end of July, 1989 generated the maximum significant wave height of 5.1 m for the 6-month period. The peak period corresponding to the largest wave was almost 8 sec. The 12-month (Aug. 1991–Jul. 1992) time series from buoy 42001 (25.9°N, 89.7°W) showed that the monthly mean significant wave heights ranged from 0.6 to 1.8 m and monthly mean peak periods from 4.3 to 5.5 sec. The monthly mean significant wave heights, which also show a decreasing trend from winter to summer months, compared reasonably well with the WIS hindcast data. Wave direction was not recorded for either time interval.

LATEX station 16 (28.9°N, 90.5°W) is located within the general study area. The wave data, recorded by MiniSpec (Coastal Leasing, Inc.) directional wave gauges during a 6-month period (Dec. 1993 and Feb.–Jun. 1994), show that the monthly-mean wave heights varied from 0.3 to 1.3 m and wave period from 5.5 to 6 sec. The dominant wave directions agree with the previous data sets showing the contribution of southeasterly approaching waves. On synthesizing these data, four scenarios are presented which represent the respective deep-water wave conditions for fairweather through severe storms—excluding hurricanes (Table 2).

Change in Wave Field due to Shoal Removal

To quantify numerically, the control that Ship Shoal exerts on wave climate, the approach taken centered on removal of the entire shoal complex from the bathymetric grid. By comparing the wave fields obtained from running the wave model over these two grids, the significance of Ship Shoal in altering

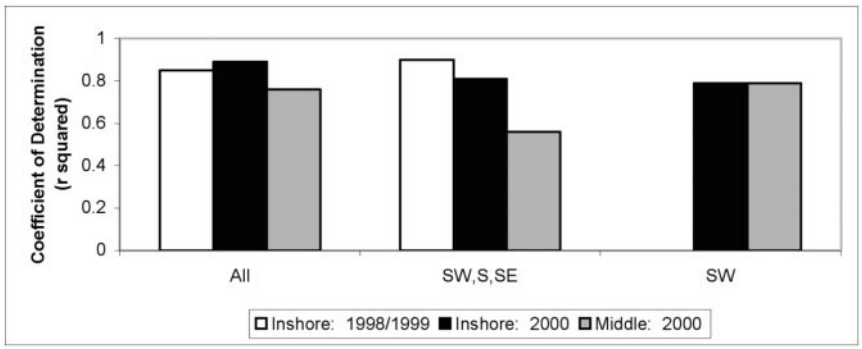

Figure 6. Summary of r^2 values for measured and modeled H_s for all stations.

Table 3. *Percentage of over prediction of H_s by STWAVE when compared to* in situ *measurements at two locations on Ship Shoal, based on 590 model runs.*

	1998/1999 Deployment (*inshore*)		2000 Deployment (*inshore*)		2000 Deployment (*Middle*)	
Wind Direction	Percentage	r^2	Percentage	r^2	Percentage	r^2
From: SW, S, SE	14.1	0.90	23.4	0.81	7.6	0.56
From: SW	No waves from this direction		19.4	0.79	6.4	0.79
All Data	24.2	0.85	23.4	0.89	13.1	0.76

wave climates under different conditions was examined. As much as a 6 m thick section of sand was removed at the west portion of the shoal, and the total volume of sand extracted from Ship Shoal was 1.1×10^9 m^3. A selection of graphs showing percentage change in significant wave height after shoal removal is presented in Figure 4. Interpretation of the data indicates that removal of Ship Shoal will alter wave propagation, dissipation and the wave energy distribution. The magnitude and spatial distribution of the alteration depend on the initial wave conditions. During severe storms (Scenario 1) and strong storms (Scenario 2), wave breaking occurs seaward of the western flank of Ship Shoal. Therefore, removal of Ship Shoal causes a maximum increase of the significant wave height by 90%–100% (*i.e.,* almost double the present value) in Scenario 1, and 40%–50% in Scenario 2, over the shoal and immediately adjacent to the lee of it. Wave breaking does not occur on the east flank of the shoal because of much deep water, and the magnitude of the wave height increase due to shoal removal is significantly less on comparison with that on the west flank. During weak storms (Scenario 3) and fair weather conditions (Scenario 4), waves do not reach breaking conditions over any part of Ship Shoal. On the west part of the shoal, the magnitudes of significant wave height increase due to shoal removal are considerably smaller, only 10%–20%. Wave height change on the east part of the shoal is minimal. Dissipation mechanisms are a combination of wave breaking over the shoal and bottom friction along deeper parts of the shoal.

The nearshore wave field is largely dependent on offshore wave conditions. Under high energy conditions in Scenario 1 and Scenario 2, removal of Ship Shoal results in higher breaking waves; however, the breaker zone is displaced between 0.5–1.0 km offshore. Ultimately, waves in the surf zone eventually attain the same energy level with and without the shoal, suggesting that shoal removal will not significantly change wave energy conditions along the Isles Dernieres. Un-

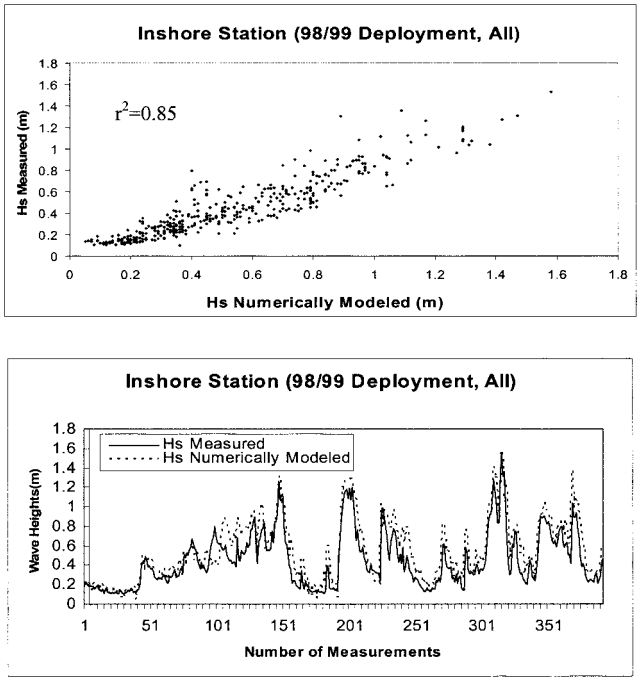

Figure 7. (upper) Scatter plot of significant wave heights for 1998/99 deployment for all wind directions at Inshore station. (lower) Comparison of measured and numerically modeled wave heights for all wind directions in 1998/99 deployment at Inshore station.

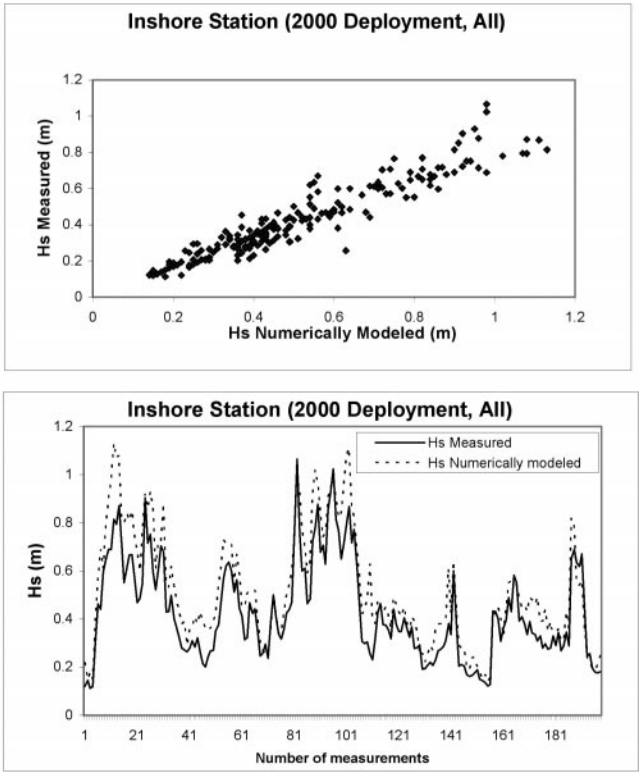

Figure 8. (upper) Scatter plot of significant wave heights for all wind direction at Inshore station for 2000 deployment. (lower) Comparison diagram of numerically modeled and measured wave heights for all wind directions at Inshore station for 2000 deployment.

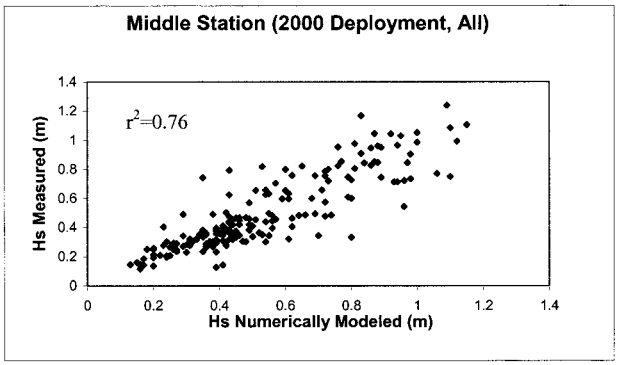

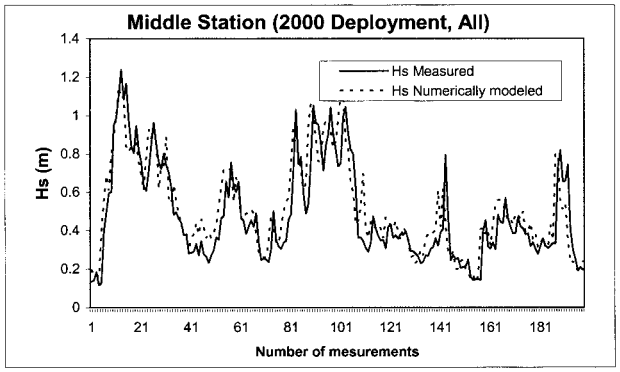

Figure 9. (upper) Scatter plot of Hs measured vs. Hs numerically modeled for 2000 deployment at Middle station. (lower) Comparison diagram of numerically modeled and measured wave heights for all wind directions at Middle station for 2000 deployment.

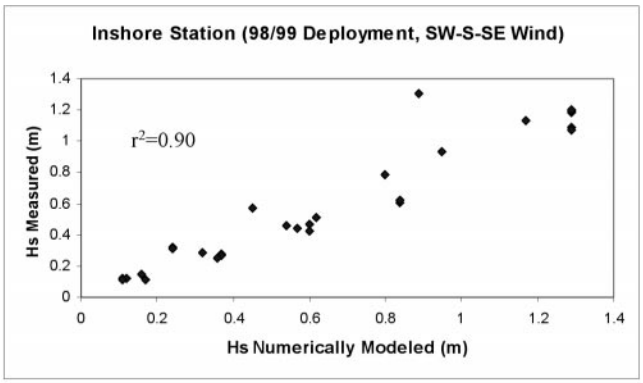

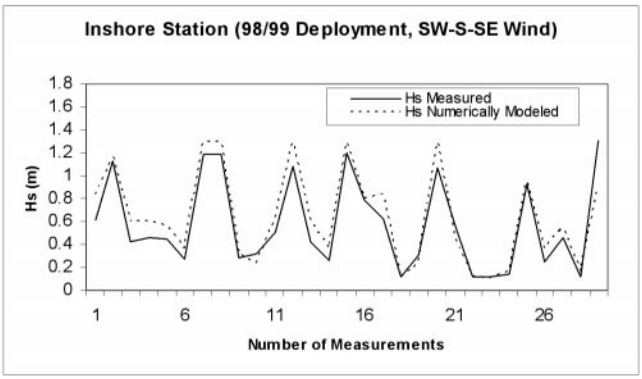

Figure 10. (upper) Scatter plot of measured and modeled H_s for wind blowing from southwest, south and southeast for 1998/99 deployment at Inshore station. (lower) Comparison diagram of numerically modeled and measured wave heights for selected southwest, south and southeast winds at Inshore station for 1998/99 deployment.

der weaker energy conditions in Scenarios 3 and 4, change in nearshore wave energy is even less noticeable particularly along the east flank of the study area.

Inclusion of a wind function increases wave height in all simulations. The magnitude of the increase is dependent on the deep water wave height and the slope of the shoreface profile. In Scenario 1, the surf zone is widened by almost 1.0 km whereas in Scenario 4, change is minimal. Removal of Ship Shoal results in a 50% increase in significant wave height. This is much larger than when wind forcing is neglected, *i.e.,* a 25–30% increase. The magnitude of wave height increase due to wind forcing over the east part of the shoal is as much as 0.8 m. Although the inclusion of the wind forcing function allows for an increase in wave height, the effects attributable to the removal of Ship Shoal are limited to the periphery of the leeward flank of the shoal, particularly along its western boundary. Changes in wave approach direction redistribute the increase in wave height in the lee of the shoal complex. This does not, however, change breaker wave heights in the nearshore along the Isles Dernieres.

Simulation of long wave propagation landward during Hurricane Andrew (STONE *et al.,* 1995) indicates near total wave energy dissipation, as opposed to breaking, over Ship Shoal. A much smaller percentage of low amplitude waves crossed the shoal complex. Peak wave energy dissipation rates occurred, however, seaward of Ship Shoal in approximately 25–30 m water depths.

Validation of STWAVE

The output from STWAVE (version 3) was tested for two bottom boundary layer field deployments conducted in 1998/1999 and 2000. Data from these deployments are presented below. Two stations were established for the first deployment (offshore and inshore on Figure 1) and a third station midway between the former during the 2000 deployment. For both deployments, wave information measured at the offshore station was selected as the input boundary condition for the model. The wind conditions for the 1998/99 deployment were obtained from Grand Isle, Louisiana, and a Terrebonne Bay site for the 2000 deployment. The input wave spectra (JONSWAP) were calculated by STWAVE from measured significant wave heights, peak wave period, wave direction and corresponding wind information. A range of 15 frequencies was applied over 35 approach angles. Peak, low, and high cut off frequencies were dependant on the individual measured wave parameters at the boundary station. Because STWAVE is a half-plane model (*i.e.,* wave energy can only

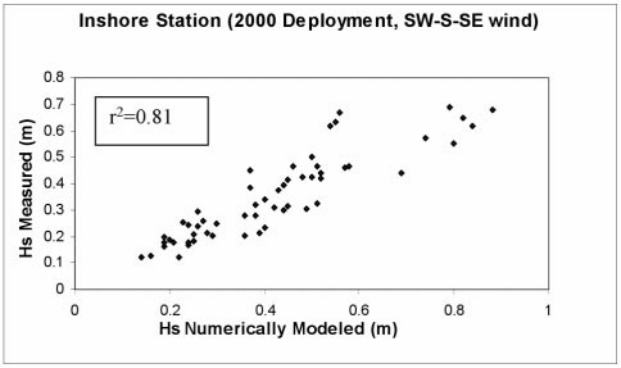

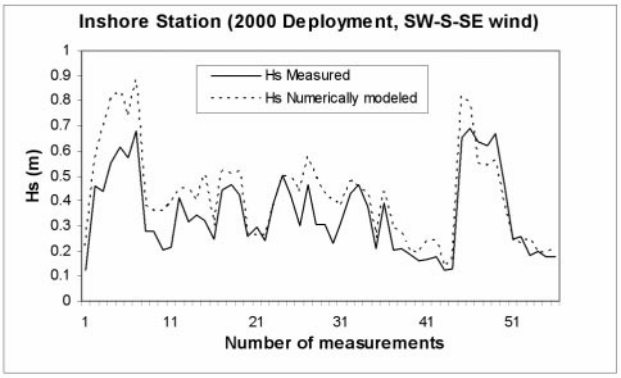

Figure 11. (upper) Scatter plot of Hs measured vs. Hs numerically modeled at Inshore station for southwest, south and southeast wind directions for 2000 deployment. (lower) Comparison diagram of numerically modeled and measured wave heights for southwest, south and southeast wind directions at Inshore station for 2000 deployment.

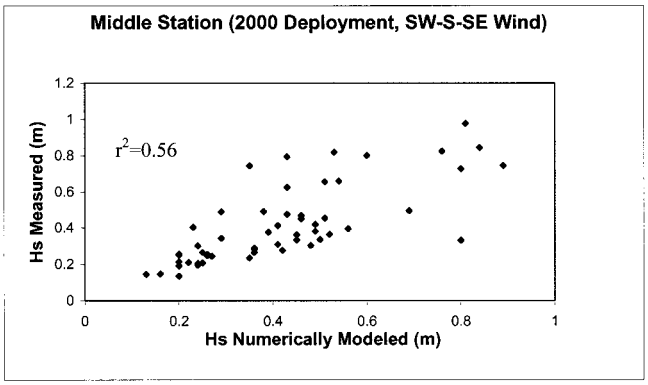

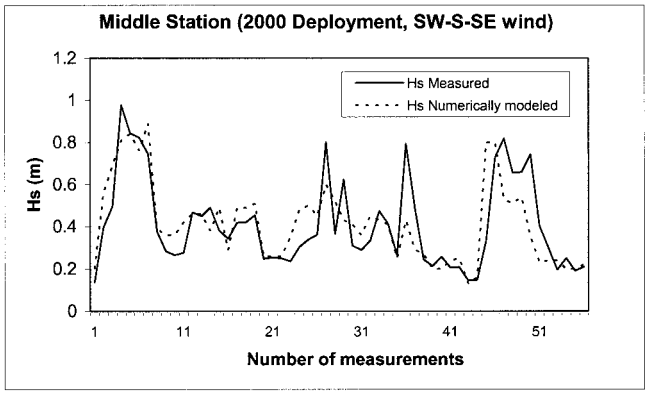

Figure 12. (upper) Scatter plot of Hs measured vs. numerically modeled Hs at Middle station for southwest, south and southeast winds foe 2000 deployment. (lower) Relationship between numerically modeled and measured significant wave heights at Middle station for southwest, south and southeast winds.

propagate from offshore to onshore or ± 87.5° from the grid × axis), wind generated waves from the north are neglected. The bathymetric grid at Ship Shoal had the dimensions 16.6 km by 27.1 km. As shown on Figure 1, the offshore station was located on the south side boundary of the modeling area, and the mid and inshore stations to the north. The bathymetric grid was generated from surveys conducted in the 1980's by the United States Geological Survey. Bathymetry for the west and northwest part of the study site was obtained from the National Ocean Service. The grid size is 166 by 271 with 100 m spacing. Measured wave and wind data were input to the model for both time series every 3 hr for the 1998/99 time series and 4 hr for the 2000 time series. A total of 590 models runs were conducted.

Comparison of Measured and Modeled Data

High r^2 values of 0.85 and 0.89 were obtained on regressing measured on numerically derived significant wave heights. The results are summarized in Figures 5 and 6 and Table 3. As shown in Figures 7 and 8, the measured and predicted values are in good agreement throughout the entire range of wave heights measured, 0.1 to 1.6 m. At both stations for each deployment, the model over predicts wave height by between 23 and 24% (Table 3). At the Middle station for the 2000 deployment, the r^2 value is 0.76 (Figure 9) for all wind directions and the percentage over prediction is 13% (Table 3) for H_s values ranging between 0.1 to 1.2 m.

Given that STWAVE does not account for waves generated and propagated from the north, input wave parameters of waves approaching from the southwest, south and southeast were extracted from the measured data sets and input to the model. For the 1998/99 deployment at the Inshore station, the r^2 value increased to 0.9 and the percentage over prediction of H_s decreased to 14.1% when compared to all data (*i.e.,* winds from all four quadrants) (Figure 10). For the 2000 deployment, however, the r^2 value decreased slightly to 0.81 and the percentage over prediction remained the same (23.4%) (Figure 11). Data obtained from the Middle station showed a marked decrease in over prediction from 13.1% down to 7.6% and a decrease in the r^2 value from 0.76 to 0.56 (Figure 12).

To test the model further, waves approaching from the southwest were extracted from the time series and used as

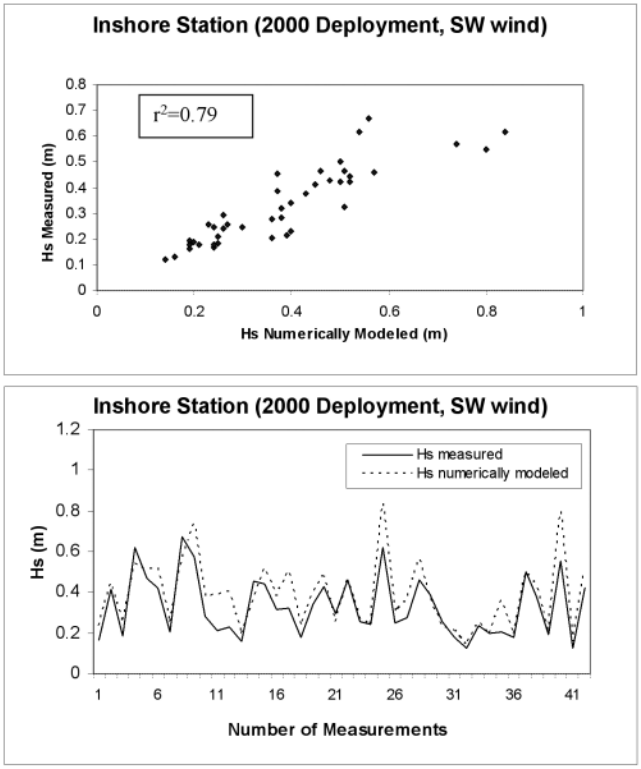

Figure 13. (upper) Scatter plot of Hs measured vs. Hs numerically modeled for south-west wind only at Inshore station for 2000 deployment. (lower) Relationship between numerically modeled and measured significant wave heights for south-west wind only at Inshore station.

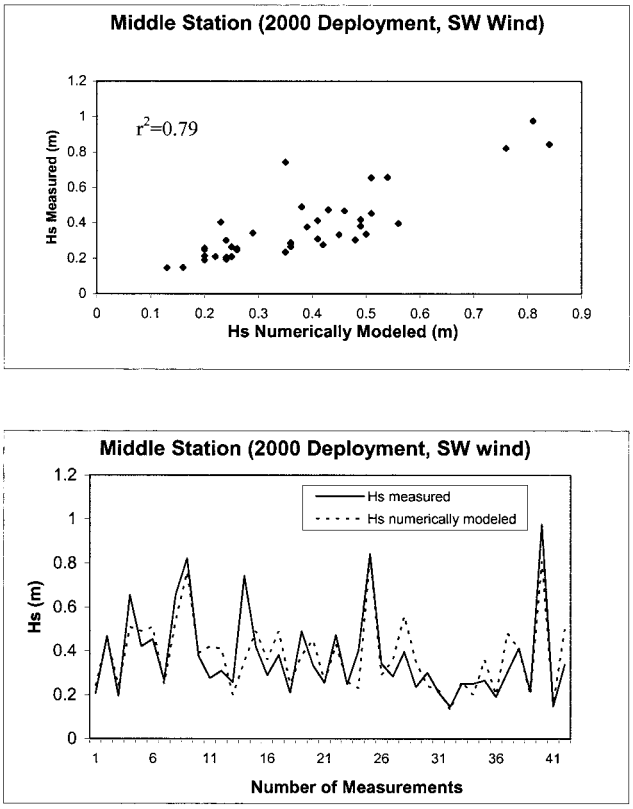

Figure 14. (upper) Scatter plot of Hs measured vs. Hs numerically modeled for south-west wind only at Middle station for 2000 deployment. (lower) Relationship between numerically modeled and measured significant wave heights for south-west wind only at Middle station.

input. This was done to test if the orientation of the instrumentation array (slightly southwest to northeast) and wave refraction effects across the seaward flank of Ship Shoal were of significance in the comparisons of data sets. During the 1998/1999 deployment waves did not approach from the southwest, a common phenomenon during winter months off the Louisiana coast. For the 2000 deployment at the Inshore station, the r^2 value decreased slightly when compared to SW, S and SE approaches from 0.81 to 0.79 (Figure 13). The percent over prediction in H_s decreased by 4% to 19.4%. At the Middle station, the r^2 value increased from 0.56 to 0.79, and the percent over prediction of H_s decreased by 1.2% to 6.4% (Figure 14).

CHANGE IN HYDRODYNAMICS AND SEDIMENT TRANSPORT

Field Measurement

In order to establish the role that Ship Shoal plays on regional hydrodynamics and sediment transport, two deployment sites were selected specifically to collect data from the seaward and landward sides of the shoal complex (Figure 1). Wind data were obtained from the Grand Isle C-Man station. Three bottom-mounted instrumentation systems were used, two of which (Systems 1A and 1B) were deployed a few meters away from each other at Site 1, while the other (System 2A) was deployed at Site 2. System 2A was retrieved on January 12, 1999, and the others remained at Site 1 until February 2, 1999. Due to memory constraints, however, System 1A ceased recording on January 20, 1999. All instrumentation was calibrated, prior to deployment, by the Louisiana State University Coastal Studies Institute Field Support Group.

The instrumentation consisted of two types of frame-mounted system, both of which included internal compasses, tilt and roll sensors, and a self-contained data recorder module. The primary components of Systems 1A and 2A (Figure 15) were SonTek™ downward-looking Acoustic Doppler Velocimeters (ADV's) that measured seabed elevation, relative particulate concentration and three-dimensional currents 20 cm above the bed. System 1A sampled at 25 Hz for 81 secs every three hours. System 2A included a Paroscientific pressure sensor in addition to the ADV, and sampled at 4 Hz for 8.5 min every 3 hr.

System 1B (called WADMAS) included a Paroscientific pressure sensor, a sonar altimeter, and a vertical array of three co-located Seapoint optical backscatter sensors (OBS's) and Marsh-McBirney electromagnetic current meters (Figure 16). WADMAS thus measured water level, directional wave

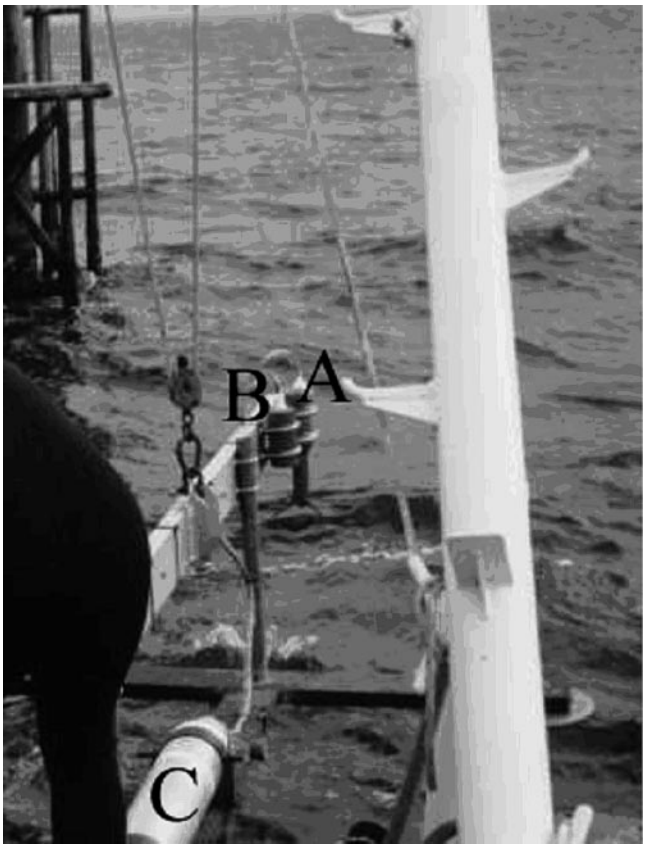

Figure 15. System 2A during deployment at Site 2. (A) Acoustic Doppler Velocimeter. (ADV) (B) Pressure Sensor. (C) Waterproof housing containing recorder module, compass and power supply. System 1A was identical except that it did not include a pressure sensor.

parameters, and seabed elevation, as well as current velocity and suspended sediment concentration at heights of 20, 60, and 100 cm above the seabed. The sonar altimeter collected one measurement every 15 min, while all other sensors sampled for 8.5 min per hour at a frequency of 4 Hz.

Hourly wind data for the deployment period were obtained from the National Oceanic and Atmospheric Administration (NOAA) station located on Grand Isle, Louisiana (GDIL1). Daily National Weather Service maps were also inspected to identify the occurrence of frontal passages. "Storm" winds associated with frontal passages are defined in this paper as those that exceeded one standard deviation above the mean wind speed for the study period, a value of 7.3 m s^{-1}. Prefrontal winds were those that blew from a direction between 90 and 270° and occurred prior to the cold front passage. The post-frontal phase included the period subsequent to the frontal passage when wind direction was between 270 and 90°.

For a detailed description of field data analysis techniques, the reader is referred to Pepper (2000); Stone (2000) and Pepper and Stone (2002), Pepper and Stone (in review). In summary, directional wave parameters were calculated from the pressure and current-meter data using the spectral method outlined by Earle *et al.* (1995). Two methods were employed to calculate an initial value of shear velocity, depending on the instrumentation system from which the data were obtained. The Reynolds stress (RS), or eddy correlation, technique was used to calculate shear velocity and apparent bottom roughness from the ADV data (Systems 1A and 2A). The logarithmic profile method (LOG) was used to calculate bottom boundary layer parameters from the System 1B data. A method based on the Grant-Madsen model (1979, 1986) was also employed on calculating shear velocity during combined waves and current flows, owing to the model's widespread familiarity and high level of empirical verification (Larsen *et al.,* 1981; Cacchione *et al.,* 1987; Huntley and Hazen, 1988).

Critical shear velocity of the bottom sediment (u_{*crit}) was calculated using a modified Yalin technique outlined by Li *et al.* (1996). This yielded a value of 0.81 cm s^{-1}, and because sediment at the study site was fairly uniform in size, it was assumed that this single value could be applied. The sediment suspension profile was represented using the standard Rouse (1937) equation because it has been demonstrated to be a fairly accurate representation for sandy environments, even under combined wave and current flows (Lynch *et al.,* 1997)

Suspended sediment transport is represented mathematically by time- and depth-integrating the product of the horizontal velocity of the fluid and the suspended sediment concentration. This is a complex problem in combined-flow regimes, owing to phase differences in velocity and concentration, and the possible occurrence of secondary flows including ejected vortices (Agrawal and Aubrey, 1992; Osborne and Greenwood, 1993; Davies, 1995). Results of this calculation are therefore very sensitive to the time-scale chosen. The method chosen here, labeled the time-averaged approach (TA), was to multiply the burst-averaged velocity and concentration profiles as calculated on the basis of the shear velocity. This approach has often been employed in wave-dominated environments (*e.g.* Vincent *et al.,* 1981; Kim *et al.,* 1997) despite the fact that it assumes temporally-uniform values, a condition that may not be satisfied during unsteady oscillatory flow. The profiles were integrated both within and above the wave boundary layer (WBL) using:

$$Q_{sn} = \begin{cases} \dfrac{1}{t}\displaystyle\int_{z=\delta_w}^{z=\eta}\int_0^t uC_n\,dz\,dt & \text{for } z > \delta_w \\ \dfrac{1}{t}\displaystyle\int_{z=z_0}^{z=\delta_w}\int_0^t uC_n\,dz\,dt & \text{for } z < \delta_w \end{cases}$$

where η is the sea surface elevation. Bed load transport rate (Q_b) was calculated by using the combined wave-current shear stress as an input to the empirical formula of Meyer-Peter and Muller (1948) as adapted by Wiberg *et al.* (1994):

$$1Q_b = 8\frac{(\tau - \tau_{crit})}{(\rho_s - \rho)g}$$

Bedload transport was assumed to occur in the same direction as that of the maximum shear stress (φ_{max}) within the WBL.

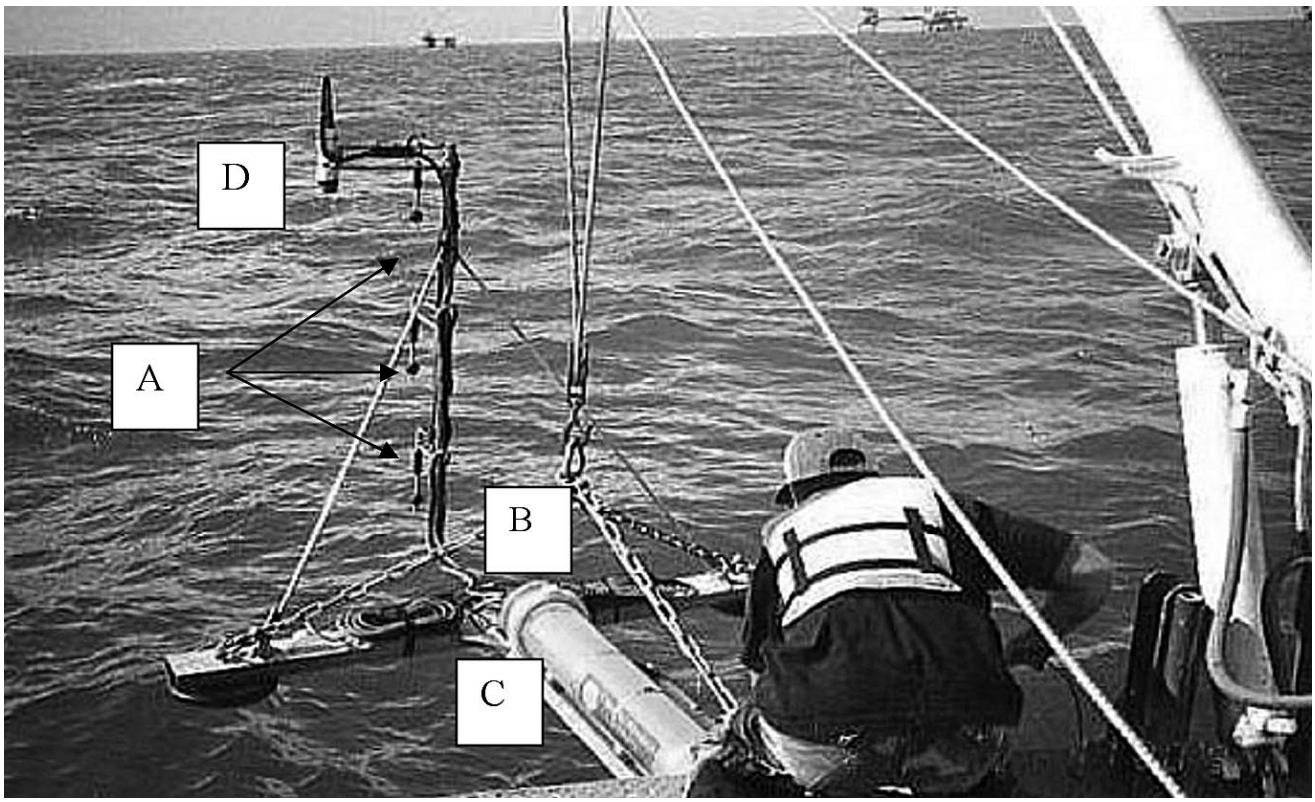

Figure 16. System 1B during deployment at Site 1. (A) Stacked array of co-located electromagnetic current meters and optical backscatter sensors. (B) Pressure Sensor. (C) Waterproof housing containing recorder module, compass and power supply. (D) Sonar altimeter.

Table 4. *Summary of hydrodynamic parameters recorded by the systems at Sites 1 and 2 during the deployment.*

Location System	Statistic	Site 1 (*offshore*) 1A (ADV)	1B (WADMAS)	Site 2 (*nearshore*) 2A (ADV)
Total Depth (m)	Mean	8.8	9.0	7.3
	Minimum	8.2	8.4	6.7
	Maximum	9.2	9.5	7.8
Hs (m)	Mean	n/a	0.61	0.45
	Minimum	n/a	0.07	0.10
	Maximum	n/a	2.80	1.53
Tp (s)	Mean	n/a	5.3	5.0
	Minimum	n/a	3.6	3.6
	Maximum	n/a	9.1	9.1
Orbital Velocity (cm s^{-1})	Mean	11.7	10.6	9.9
	Minimum	2.6	0.8	0.0
	Maximum	35.9	53.1	36.5
Current Speed (cm s^{-1}) (~0.2m above bed)	Mean	5.8	4.6	6.3
	Minimum	0.1	0.1	0.0
	Maximum	44.8	34.2	47.6
Current Speed (cm s^{-1}) (~1 m above bed)	Mean	12.4	8.0	13.9
	Minimum	0.1	0.1	0.0
	Maximum	72.4	53.2	62.3
Current Direction	Mean	245	240	292

Influence of Ship Shoal on Hydrodynamics and Sediment Transport

Table 4 is a summary of hydrodynamic parameters for the deployment. Points to note include the depth, which was 1.5–2.0 m deeper offshore (Site 1) than nearshore (Site 2), and the depth range, which was slightly greater than 1.0 m at both sites. Significant wave height and wave orbital velocity were higher at Site 1 than at Site 2, by 36 and 18%, respectively, which is consistent with the expectation that waves crossing Ship Shoal are attenuated as a result of bottom friction. Because of the attenuation of swell waves propagating northward across the shoal, peak wave period was 9% lower at the nearshore site, where locally-generated sea assumed a greater relative importance.

Differences in current velocity between sites were less expected and are less easily explained than differences in wave parameters. In contrast to wave energy, mean current speed was approximately 10% higher at Site 2 (nearshore) than Site 1 (offshore). Current direction had a strong westerly component at both sites, which is consistent with previous research (Crout and Hamiter, 1981; Murray, 1997; Jaffe *et al.*, 1997). However, the across-shelf current component was seaward at the offshore site and landward at the nearshore site (Figure 17). Since the two sites are separated by only a few kilometers and are subject to similar atmospheric and tidal

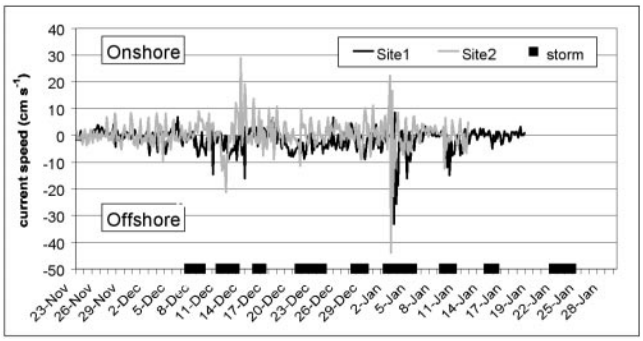

Figure 17. Across-shelf current flow during the deployment at Sites 1 and 2 (at ~20 cm above the bed) as measured by Systems 1A and 2A.

forcing mechanisms, this was apparently the result of flow modulation by Ship Shoal's bathymetry. A likely explanation is that the prevailing westward currents were steered downslope by gravity on opposite sides of the shallow shoal, resulting in southward flow at Site 1 and northward flow at Site 2. Although this is difficult to verify using the available data set, preliminary results from a recent deployment suggest that this interpretation is correct. Ship Shoal controls the regional hydrodynamics, a phenomenon that is presumably also significant on any inner shelf that includes submerged sand bodies or other prominent bathymetric features. Furthermore, this influences bottom boundary layer dynamics and sediment transport on the Louisiana inner shelf, a point that will be discussed further in the context of cold front passages.

Significance of Cold Front Passages

Nine cold front passages occurred during the deployment, or approximately one per week. Overall, mean wind speed and direction were 8.1 m s^{-1} and 354° (northerly) during storm periods and 3.8 m s^{-1} and 113° (southeasterly) during fair weather. Clockwise rotation (veering) of the wind from south to north was typical during frontal passages.

The cospectrum of across-shelf winds and currents (Figure 18) shows a positive peak at periods of 5 to 10 days (which is statistically-significant at a 90% confidence level). The phase spectrum (Figure 18) indicates that there was little phase difference between wind and current variability. The same was true of along-shelf winds and along-shelf currents, although the cospectrum was not statistically significant over most frequencies. Thus, southerly winds were generally coincident with northerly currents, and northerly winds were coincident with southerly currents, with cold-front passages apparently providing the major energy input.

Cold-front passages had a strong influence on inner-shelf hydrodynamics. Wave height increased steeply as did mean and oscillatory currents (Figures 19A and B). Mean and wave-driven flow speeds were similar overall, although each attained a relatively higher level at different times during the deployment, likely as a result of differing meteorological forcing mechanisms.

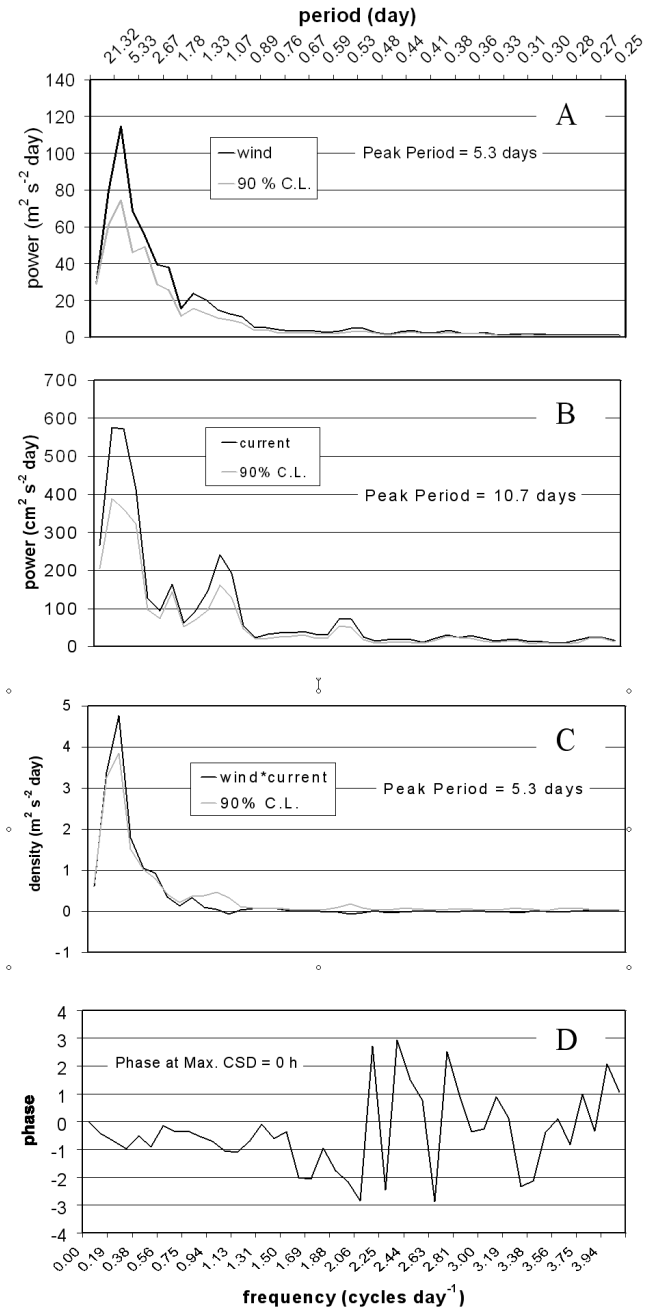

Figure 18. (A and B): Cospectrum of across-shelf wind and current. (C) Phase spectrum of wind and current. (D) CSD denotes cross-spectral density. The 90% confidence level (CL) is shown on plot s A, B and C.

Hydrodynamic differences between cold-front passages and fair weather led to differences in bottom boundary layer parameters and sediment transport, as summarized in Table 5. Episodic increases in current- and wave-current shear velocity were associated with storms, when values were generally at least 50% higher than those during fair weather conditions. Sediment transport predictions varied widely depending on the method used, and as such, they should be used

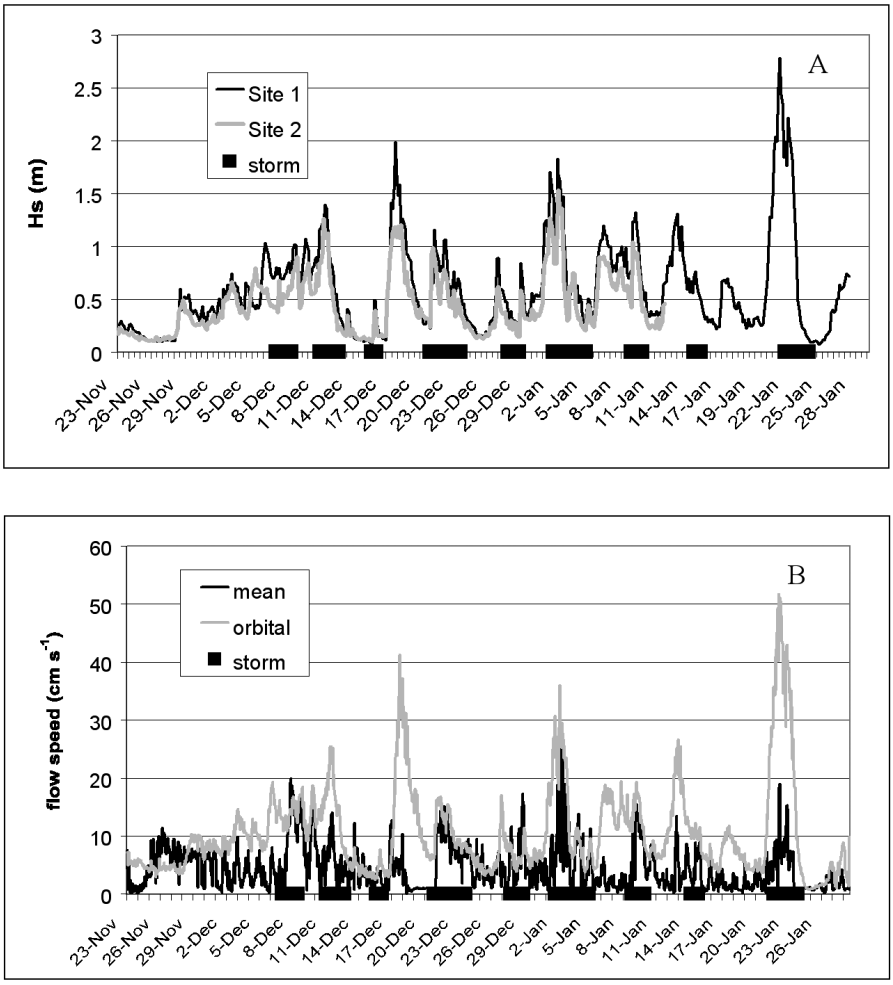

Figure 19. (A) Significant wave height at Sites 1 and 2 during the deployment period. (B) Mean and orbital (oscillatory) flow speed for Site 1. Trends were similar at Site 2.

primarily as relative estimates for the purposes of comparison. However, all estimates indicate that sediment transport in the across- and along-shelf directions was episodically increased by storms. It should also be noted, that rate of sediment transport during fair weather conditions was not predicted to be zero.

Sediment transport direction was especially variable as a result of the occurrence of different types of weather conditions. Predicted fair weather transport was westerly at Site 1, and easterly at Site 2, with the across-shelf vector tending to be onshore at both sites. Mean extratropical storm transport was offshore at both sites, with an easterly component

Table 5. *Summary of flow, bottom boundary layer (BBL), and sediment transport values during extratropical storms and fair weather conditions for Sites 1 and 2.*

	Flow Speed (cm s^{-1})		BBL Shear Velocity (cm s^{-1})		Sediment Transport (mg cm^{-1} s^{-1})			
					TA		MPM	
	Mean	Orbital	u^*_c	u^*_{cw}	Rate	Direction	Rate	Direction
Site 1								
Storms	7.5	11.4	1.7	2.7	549.1	139	97.8	145
Fair Weather	3.5	8.3	1.1	1.9	138.7	298	85.6	253
Site 2								
Storms	10.3	12.3	2.1	3.2	810.7	182	412.9	256
Fair Weather	5.1	9.2	1.6	2.5	584.8	50	325.0	17

Table 6. *Mean wave characteristics for the storm types as measured at Sites 1 and 2, respectively.*

	Site 1			Site 2		
Storm Type	Hs (m)	Tp (s)	Ub (cm s^{-1})	Hs (m)	Tp (s)	Ub (cm s^{-1})
1	0.80	4.11	12.7	0.60	3.8	12.58
2	1.06	5.82	19.1	0.66	5.0	14.29

at Site 1 and a westerly component at Site 2. However, there was considerable variability between individual cold front passages (PEPPER and STONE, 2002), and as such, a classification system was introduced.

Cold Front Classification

The classification system consisted of two end-member types on a continuum of regional cold front passages. It was determined that three cold front passages that occurred during this deployment fit into each of the two categories, and a summary of hydrodynamic and sediment transport measurements for each are presented here. More detailed results based on this classification system are discussed for two specific cold front passages by PEPPER and STONE (2002).

Type 1 storms, or arctic surges, have a weak pre-frontal phase followed by a fairly powerful post-frontal phase, during which northeasterly winds dominate. Type 2 storms are migrating cyclones dominated by a strong low-pressure cell, and have fairly strong southerly winds prior to the frontal passage, followed by strong northwesterly winds subsequent to it.

Table 6 shows wave characteristics at both sites for each of the storm types. Wave energy, as indicated both by wave height and near-bed orbital velocity, was highest at each site during Type 2 storms, followed by Type 1 storms. Wave period was considerably higher for Type 2 than for Type 1 storms.

Time series of significant wave height and peak wave period for representative Types 1 and 2 storms (Storms 6 and 7) are shown in Figures 20 and 21. Type 1 storms were characterized by an increase in significant wave height and an accompanying decrease in peak wave period associated with the onset of northerly post-frontal winds. On the other hand, wave response to Type 2 storms, as illustrated by data from Storm 6 (Figure 21), was more complex. The time series of significant wave height had two peaks, the lower of which occurred immediately prior to the frontal passage, while the higher occurred just subsequent to it. Maximum hourly significant wave height (H_s) during this event was 1.83 m and H_s exceeded 1.5 m for 10 hr around the peak of the storm. Peak wave period increased gradually to approximately 8 sec prior to the frontal passage, following which, it suddenly decreased to 3.76 sec. It then fluctuated between the high- and low-frequency values for 24 hr, at which point it leveled off at approximately 4 sec.

The directional characteristics of waves associated with various phases of the two storm types provide additional information regarding their dynamics and generating mechanism. Figures 22 and 23 are vector plots of non-dimensional wave direction during Types 1 and 2 storms, respectively. In both cases, wave direction was uniformly toward the northwest during the pre-frontal stage. Immediately following the passage of the front, however, wave direction differed between storm types—in the case of the Type 1 storm, there was an immediate shift to southerly waves, while wave direction during the Type 2 storm oscillated between northeasterly and southeasterly before ultimately aligning with the (northerly) wind direction approximately 24 h later. It should be noted that this does not indicate sudden (*i.e.* hourly) shifts in wave direction, but instead, minor changes in the relative energy level of the longer- and shorter-period wave bands. This is indicative of the continued importance of longer-period waves throughout the duration of Type 2 storms.

The storm types differed in terms of their associated wave characteristics. Type 2 storms appear to have had the most energetic wave field overall, particularly during the pre-frontal phase. Significant contributions to the energy spectrum resulted from both long-period northerly swell waves, and

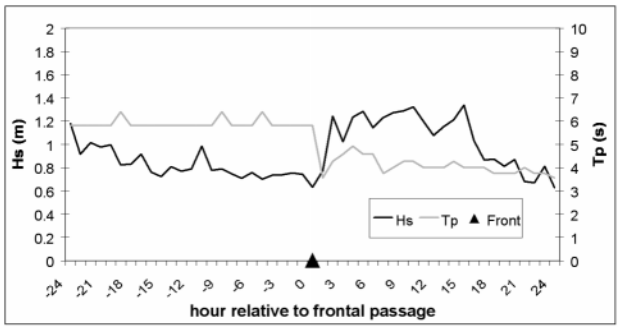

Figure 20. Significant wave height (Hs) and peak wave period (Tp) at Site 1 during a Type 1 storm (Storm 7).

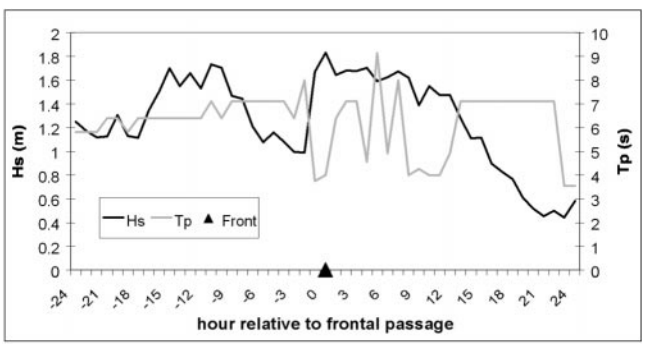

Figure 21. Significant wave height (Hs) and peak wave period (Tp) at Site 1 during a Type 2 storm (Storm 6).

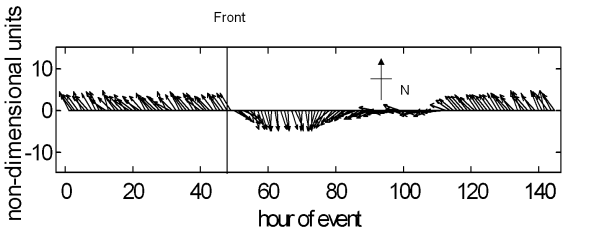

Figure 22. Non-dimensional wave direction during Storm 7, a Type 1 storm. The time of the frontal passage is indicated by the line at hour 48.

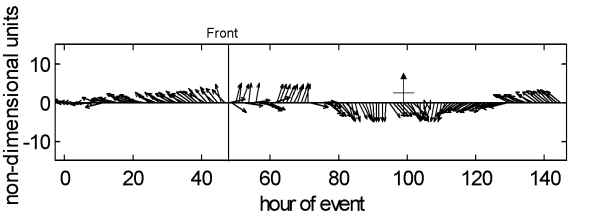

Figure 23. Non-dimensional wave direction during the Type 2 storm. The time of the frontal passage is indicated by the vertical line at hour 48.

short-period, southerly storm waves, both of which were present during the majority of the post-frontal phase. Type 1 storms, on the other hand, were dominated by short-period southerly waves subsequent to the frontal passage. As outlined above, Type 1 storms were characterized by weak southerly pre-frontal winds and energetic northerly pre-frontal winds, thus resulting in higher southerly post-frontal storm waves. In contrast, the strong southerly pre-frontal winds that accompanied Type 2 storms acted over a larger fetch than was present during periods of northerly winds, resulting in the generation of northerly long-period waves that were energetic enough to persist throughout much of the storm. This also explains the relative reduction in significant wave height and peak wave period at Site 2 during Type 2 storms, since northerly, and not southerly, waves are primarily influenced by attenuation across Ship Shoal at this site.

Table 7 shows mean currents for the storm types based on the field deployment data. Overall and post-frontal current speeds were highest during Type 1 storms, although during the pre-frontal phases, current speed was nearly twice high during Type 2 storms. Mean current direction during this phase was northwesterly for both storm types. The (stronger) post-frontal currents were southwesterly during Type 1 storms, and southeasterly during Type 2 storms, which is closely reflected in the overall current direction for these events. The absence of strong currents prior to the frontal passage was likely the result of the fairly weak winds that predominated during the pre-frontal phase of Type 1 storms. Similarly, the powerful southeasterly or southwesterly post-frontal currents observed immediately following the frontal passages were probably the result of strong, direct wind stress during the post-frontal phase.

Standard bottom boundary layer parameters for Site 1, calculated by applying the logarithmic profile (LOG) method to current data from System 1B, are presented in Table 8. The results obtained by applying the Reynolds Stress (RS) method to the 3-D current data from Systems 1A and 2A are not presented here, largely owing to the smaller data sets available, and the fact that general trends apparent from these systems were similar. Shear velocity was almost identical overall during Types 1 and 2 storms. During the 24 hours prior to the frontal passage, however, shear velocity was much higher for Type 2 than for Type 1 storms. Calculated shear velocity values were higher during the post-frontal than the pre-frontal phase for both types of storms, with Type 2 storms again being characterized by the highest values. Apparent bottom roughness was clearly highest during Type 2 storms. The reasons for this are unclear, although it is possible that high wave activity occurring during the pre-frontal phase of Type 2 storms created physical bed roughness elements such as wave ripples. These may have been absent, or at least less prominent, during the other storm type, and additionally, may have been washed out by strong post-frontal currents during Type 1 storms.

Table 9 summarizes the overall suspended and bed load transport estimates for Sites 1 and 2 during the three storm types, as estimated using the time-averaged (TA) and Meyer-Peter and Muller (MPM) methods, respectively. It is evident that at both sites, and according to both methods, Type 2 storms were responsible for the largest rates of sediment transport, while Type 1 storms had transport rates several times lower. Both suspended and bed load sediment transport direction ranged between southerly and westerly during Type 1 storms, depending on the prediction method used and the location. Transport had a stronger offshore component at Site 1, where the overall direction was nearly southerly, than at Site 2, where transport was predominantly westerly. Suspended sediment transport during Type 2 storms was toward the southeast; however, unlike Type 1 storms, there was a stronger offshore component at Site 2 than at Site 1. Bed load transport during Type 2 storms was southwesterly at Site 1, and southeasterly at Site 2. In summary, therefore, sediment transport rate during Type 1 storms was not as high as dur-

Table 7. *Mean current parameters for the storm types as measured at approximately 1 m above the bed by System 1B at Site 1.*

	Storms		Pre-frontal		Post-frontal	
Storm Type	Speed (cm s^{-1})	Direction	Speed (cm s^{-1})	Direction	Speed (cm s^{-1})	Direction
1	16.5	229	5.8	315	17.4	228
2	13.2	141	11.7	287	17.2	123

Table 8. *Current-induced and combined wave-current shear velocity (u^*_c and u^*_{cw}, respectively), and apparent bottom roughness (z_o) for the storm types at Site 1.*

	All Storm Conditions			Pre-frontal (24 h)			Post-frontal (24 h)		
Storm Type	u^*_c (cm s^{-1})	u^*_{cw} (cm s^{-1})	z_0 (cm)	u^*_c (cm s^{-1})	u^*_{cw} (cm s^{-1})	z_0 (cm)	u^*_c (cm s^{-1})	u^*_{cw} (cm s^{-1})	z_0 (cm)
1	1.51	2.55	1.66	0.63	1.15	3.37	1.52	2.57	1.63
2	1.52	2.55	4.11	1.23	2.43	4.09	2.01	3.22	4.07

ing Type 2 storms, and the mean direction tended to be southwesterly at Site 1 and westerly at Site 2, while during Type 2 storms, mean sediment transport was directed southeasterly at Site 1, and southerly at Site 2.

CONCLUSIONS

Ship Shoal mitigates the adjacent wave field off the Louisiana coast, particularly during storm conditions. The interaction of fairweather waves with the shoal is negligible. Removal of the shoal, however, for possible future barrier/coastal restoration efforts will not significantly influence wave conditions in the nearshore because the expected increase in wave energy is limited to the leeward flank of the shoal. The data presented indicate that STWAVE over predicts H_s by between 6 and 24%. Over prediction shows a general decrease when winds from the northern two quadrants are removed from the time series. Modeling waves propagating from the southwest to incorporate possible refraction across the shoal does not significantly alter either the over prediction percentage or r^2 value when compared to wave approaches from both southern quadrants. Overall, the model has predicted H_s satisfactorily over a broad spectrum of wave conditions for the northern Gulf of Mexico.

Hydrodynamic, bottom boundary layer, and sedimentary processes on the Louisiana inner shelf during the winter are characterized by episodic variability, largely as a result of the quasi-periodic cycle of recurring cold front passages. Specifically, these events are characterized by increases in wave height, oscillatory and mean current speed, shear velocity, and sediment transport. Waves tend to be higher and longer in period on the seaward side, whereas mean currents are generally higher landward, where they are directed onshore, unlike the offshore site, where seaward currents predominate. Sediment transport initiated by cold fronts is generally directed southeasterly to southwesterly at the offshore site, and southerly to westerly at the nearshore site. It is clear, therefore, that Ship Shoal exerts a significant influence on regional hydrodynamics and sediment transport.

End-member cold front types can be identified. Type 1 storms are arctic surges that are associated with southerly storm waves, and southwesterly to westerly currents and sediment transport. Type 2 storms are migrating cyclones that cause northerly swell that transforms into southerly sea, and currents and sediment transport that are southeasterly overall.

ACKNOWLEDGEMENTS

Funding for this work was obtained from the U.S. Minerals Management Service under contracts 14-35-0001-30660 and 14-35-0001-30660-19911b. We thank Dr. Don Resio (Coastal and Hydraulics Laboratory), and Dr. James Kirby (University of Delaware) for helpful discussion on STWAVE and REF/DIF S respectively. Cartographic assistance was obtained from Mary Lee Eggart, Kerry Lyle and Clifford Duplechin (Louisiana State University). We acknowledge the constructive criticisms offered by Drs. Nick Kraus and Alexis Lugo-Fernandez on an earlier draft of this manuscript. The Coastal Studies Institute's Field Support Group at LSU performed all array mount fabrication and deployment.

LITERATURE CITED

ABEL, C.E.; TRACY, B.A.; VINCENT, C.L., and JENSEN, R.E., 1989. Hurricane Hindcast Methodology and Wave Statistics for Atlantic and Gulf Hurricanes from 1956–1975. USAE Waterways Experiment Station, Vicksburg, MS, *WIS Report 19,* 33 p.

AGRAWAL, Y.C. and AUBREY, D.G., 1992. Velocity Observations Above a Rippled Bed Using Laser Doppler Velocimetry. *Journal of Geophysical Research,* 97(C12), 20249–20259.

BRITSCH, L. D. and DUNBAR, J. B., 1993. Land loss rates: Louisiana coastal plain. *Journal of Coastal Research,* 9, 324–338.

BYRNES, M.R. and GROAT, C. (eds.), 1991. Characterization of the Development Potential of Ship Shoal Sand for beach Replenishment of the Isles Dernieres. Final Report to the U.S. Minerals Management Service, 164 p.

CACCHIONE, D.A.; GRANT, W.D.; DRAKE, D.E., and GLENN, S.M., 1987. Storm-Dominated Bottom Boundary Layer Dynamics on the Northern California Continental Shelf: Measurements and Predictions. *Journal of Geophysical Research.* 92(C2), 1817–1827.

Table 9. *Sediment transport predicted with the TA and MPM methods for Systems 1A and 2A using the Reynolds stress technique for calculating shear stress.*

	Site 1				Site 2			
	TA		MPM		TA		MPM	
Storm Type	Q_b (mg cm^{-1} s^{-1})	Dir.	Q_b (mg cm^{-1} s^{-1})	Dir.	Q_b (mg cm^{-1} s^{-1})	Dir.	Q_b (mg cm^{-1} s^{-1})	Dir.
1	289.2	195	144.7	190	175.8	273	173.9	259
2	1095.6	120	388.1	118	1871.8	171	847.8	205

COLEMAN, J.M.; ROBERTS, H.H., and STONE, G.W., 1998. Mississippi River Delta: An Overview. *Journal of Coastal Research,* 14, 3, 698–716.

CROUT, R.L. and HAMITER, R.D., 1981. Response of Bottom Waters on the West Louisiana Shelf to Transient Wind Events and Resulting Sediment Transport. *Transactions of the Gulf Coast Association of Geological Societies,* 31, 273–277.

DAVIES, A.G., 1995. Effects of unsteadiness on the suspended sediment flux in co-linear wave-current flow. *Continental Shelf Research,* 15(8), 949–979.

EARLE, M.D.; MCGEHEE, D., and TUBMAN, M., 1995. Field Wave Gaging Program, Wave Data Analysis Standard. Vicksburg, Mississippi: *U.S. Army Corps of Engineers Instruction Report CERC*-95-1, 33p.

FRAZIER, D.E., 1967. Recent Deposits of the Mississippi River, their Development and Chronology. *Transactions of the Gulf Coast Association of Geological Societies,* 17, p. 287–311.

GRANT, W.D. and MADSEN, O.S., 1979. Combined Wave and Current Interaction with a Rough Bottom. *Journal of Geophysical Research,* 84(C4), 1797–1807.

GRANT, W.D. and MADSEN, O.S., 1986. The Continental-Shelf Bottom Boundary Layer. *Annual Review of Fluid Mechanics,* 18, 265–305.

GRYMES, J. and STONE, G.W., 1995. A review of the key meteorological and hydrological aspects of Hurricane Andrew. *In:* STONE, G.W. and FINKL, C.W., (eds.), Impacts of Hurricane Andrew on the Coastal Zones of Florida and Louisiana: 22–26 August 1992 *Journal of Coastal Research, Special Issue 21,* 6–23.

HOLTHUIJSEN, L.H.; BOOIJ, N., and HEBERS, T.H.C., 1989. A Prediction Model for Stationary, Short-Crested waves in Shallow Water with Ambient Currents. *Coastal Engineering,* 13, p. 23–54.

HUBERTZ, J. M. and BROOKES, R.M., 1989. Gulf of Mexico hindcast wave information. WIS report 18. *US Army Corps of Engineer, Waterways Experiment Station,* Vicksburg, MS.

HUNTLEY, D.A. and HAZEN, D.G., 1988. Seabed Stresses in Combined Wave and Steady Flow Conditions on the Nova Scotia Continental Shelf: Field Measurements and Predictions. *Journal of Physical Oceanography,* 18, 347–362.

JAFFE, B.E.; LIST, J.H., and SALLENGER, A.H., JR., 1997. Massive sediment bypassing on the lower shoreface offshore of a wide tidal inlet–Cat Island Pass, Louisiana. *Marine Geology,* 136, 131–149.

KIM, S.-C.; WRIGHT, L.D., and KIM, B.-O. 1997. The combined effects of synoptic scale and local-scale meteorological events on bed stress and sediment transport on the inner shelf of the Middle Atlantic Bight. *Continental Shelf Research,* 17(4), 407–433.

LARSEN, L.H.; STERNBERG, R.W.; SHI, N.C.; MARSDEN, M.A.H., and THOMAS, L., 1981. Field investigations of the threshold of grain motion by waves and currents. *Marine Geology,* 42, 105–132.

LI, M.Z.; WRIGHT, L.D., and AMOS, C.L., 1996. Predicting ripple roughness and sand resuspension under combined flows in a shoreface environment. *Marine Geology,* 130, 139–161.

LIST, J.H. and HANSEN, M.E., 1992. The Value of Barrier Islands: 1. Mitigation of Locally-generated Wind-Wave Attack on the Mainland. *USGS Open File Report* 92-7222, 18 pp.

LIST, J.H.; JAFFEE, B.E.; SALLENGER, A.H., and HANSEN, M.E., 1997. Bathymetric comparisons adjacent to the Louisiana barrier islands: Processes of large-scale change. *Journal of Coastal Research,* 13, 3, 670–678.

LYNCH, J.F.; GROSS, T.F.; SHERWOOD, C.R.; IRISH, J.D., and BRUMLEY, B.H., 1997. Acoustical and optical backscatter measurements of sediment transport in the 1988–1989 STRESS experiment. *Continental Shelf Research,* 17(4), 337–366.

MEYER-PETER, E. and MULLER, R., 1948. Formulas for bed-load transport. International Association for Hydraulic Structural Research, Meeting 2, Stockholm, Sweden.

MOSSA, J., 1988. Analysis of the Environmental Effects of Sand resource Utilization on the Louisiana Continental Shelf. Open-File Series No. 88-01. *Louisiana Geological Survey,* Baton Rouge, LA.

MULLER, R.A. and STONE, G.W., 2001. A climatology of tropical storm and hurricane strikes to enhance vulnerability prediction for the southeast U.S. coast. *Journal of Coastal Research,* 17, 4, 949–956.

MURRAY, S.P., 1997. An observaytional study of the Mississippi-Atchafalaya coastal plume: Final report. OCS Study MMS 98-0040. U.S. Dept. of the Interior, Minerals Management Service, Gulf of Mexico OCS Region, New Orleans, La. 513 pp.

MCBRIDE, R.A.; PENLAND, S.; HILAND, M.; WILLIAMS, S.J.; WESTPHAL, K.A.; JAFFE B., and SALLENGER, A.H. JR., 1992. Analysis of barrier shoreline change in Louisiana from 1853 to 1989. *In:* WILLIAMS, S.J. *et al.* (eds.), Atlas of Barrier Island Changes in Louisiana from 1853 to 1989. *USGS Miscellaneous Investigations Series* I-2150-A, 36–97.

MCBRIDE, R.A. and BYRNES, M.R., 1997. Regional variations in shore response along barrier island systems of the Mississippi River delta plain: Historical change and future prediction. *Journal of Coastal Research,* 13, 3, 628–655.

OSBORNE, P.D. and GREENWOOD, B., 1993. Sediment suspension under waves and currents: time scales and vertical structure. *Sedimentology,* 40: 599–622.

O'REILLY, W.C. and GUZA, R.T., 1993. A Comparison of Spectral Models in the Southern California Bight. *Coastal Engineering,* 17.

PENLAND, S. and SUTER, J.R., 1988. Barrier island erosion and protection in Louisiana: A coastal geomorphological perspective. *Transactions of the Gulf Coast Association of Geological Societies,* 38, 331–342.

PENLAND, S.P.; SUTER, J.R., and BOYD, R., 1985. Barrier Island Areas Along Abandoned Mississippi River Deltas. *Marine Geology,* 63, 197–233.

PENLAND, S.; SUTER, J.R., and MOSLOW, T.F., 1986. Inner-shelf shoal sedimentary facies and sequences: Ship Shoal, northern Gulf of Mexico, *In:* MOSLOW, T.F. and RHHODES, E.G., eds., Modern and ancient shelf clastics: A core workshop: *Tulsa, Oklahoma, Society of Economic Paleontologists and Mineralogists Core Workshop* No. 9, p. 73–123.

PEPPER, D.A., 2000. Hydrodynamics, Bottom Boundary Layer Processes, and Sediment Transport on the South-Central Louisiana Shelf: The Influence of Extratropical Storms and Bathymetric Modification. Unpublished Dissertation, Louisiana State University, Baton Rouge, 159 p.

PEPPER, D.A. and STONE, G.W., 2002. Atmospheric forcing of fine-sand transport on a low-energy inner shelf: south-central Louisiana, USA. *Geo-Marine Letters,* 22, 331–41.

PEPPER, D.A. and STONE, G.W., in review. Hydrodynamic, Bottom Boundary Layer and Sedimentary Responses to Two Contrasting Winter Storms on the Low-Energy Inner Shelf of the Northern Gulf of Mexico, *Marine Geology.*

ROUSE, H., 1937. Modern conceptions of the mechanics of fluid turbulence. *Transactions of the American Society of Civil Engineers,* 102, 463–554.

STONE, G.W., 2000. Wave climate and bottom boundary layer dynamics with implications for offshore sand mining and barrier island replenishment in South-Central Louisiana. OCS Study MMS 2000-053, 90 pp.

STONE, G.W. and PENLAND, S., 1992. Historic Shoreline Change along the Northern Gulf of Mexico. *In:* MAJUMDAR, S.K.; FORBES, G.S.; MILLER, E.W., and SCHMALZ, R.F. (eds.), Natural and Technological Disasters: Causes, Effects and preventive Measures, *The Pennsylvania Academy of Science.*

STONE, G.W. and XU, J., 1996. Wave climate modeling and evaluation relative to sand mining on Ship Shoal, offshore Louisiana, for coastal restoration and barrier island restoration. OCS Study MMS 960059, 170 pp.

STONE, G.W. and MCBRIDE, R.A., 1998. Louisiana barrier islands and their importance in wetland protection: Forecasting shoreline change and subsequent response of wave climate. *Journal of Coastal Research,* 14, 3, 900–915.

STONE, G.W.; XU, J.P., and ZHAN, G.X., 1995. Estimation of the wave field during Hurricane Andrew and morphological change along the Louisiana coast, *In:* Impacts of Hurricane Andrew on the Coastal Zones of Florida and Louisiana: 22–26 August 1992 *Journal of Coastal Research,* Special Issue 21, STONE, G.W. and FINKL, C.W. (eds.), 234–253.

STONE, G.W.; WILLIAMS, S.J., and BURRUSS, A.E., 1997. Louisiana's barrier islands: An evaluation of their geological evolution, mor-

phodynamics and rapid deterioration. *Journal of Coastal Research,* 13, 3, 591–592.

STONE, G.W.; GRYMES, J.; ROBBINS, K.D.; UNDERWOOD, S.G.; STEYER, G.D., and MULLER, R.A., 1993. A chronologic overview of climatological and hydrological aspects associated with Hurricane Andrew and its morphological effects along the Louisiana coast, USA. *Shore and Beach,* 61, 2, 2–12.

VINCENT, C.E.; SWIFT, D.J.P., and HILLARD, B., 1981. Sediment transport in the New York Bight, North American Atlantic Shelf. *Marine Geology,* 42, 369–398.

WIBERG, P.L.; DRAKE, D.E., and CACCHIONE, D.A., 1994. Sediment resuspension and bed armoring during high bottom stress events on the northern California inner continental shelf: measurements and predictions. *Continental Shelf Research,* 14(10/11), 1191–1219.

WILLIAMS, S. J.; PENLAND, S., and SALLENGER, A. H., JR., 1992. Louisiana barrier island erosion study: Atlas of shoreline changes in Louisiana from 1853 to 1989. *USGS Miscellaneous Investigations Series I*-2150-A, 103 p.

WILLIAMS, S.J.; STONE, G.W. and BURRUS, A.E., 1997. A perspective on the Louisiana wetland loss and coastal erosion problem. *Journal of Coastal Research,* 13, 3, 593–594.